

Improved Performance of the Silicon Anode for Li-Ion Batteries: Understanding the Surface Modification Mechanism of Fluoroethylene Carbonate as an Effective Electrolyte Additive

Chao Xu,[†] Fredrik Lindgren,[†] Bertrand Philippe,[‡] Mihaela Gorgoi,[§] Fredrik Björefors,[†] Kristina Edström,[†] and Torbjörn Gustafsson^{*,†}

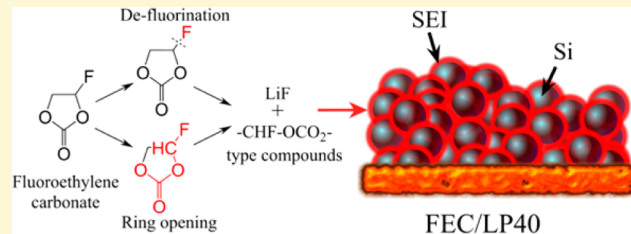
[†]Department of Chemistry - Ångström Laboratory, Uppsala University, Box 538, SE-75121 Uppsala, Sweden

[‡]Department of Physics and Astronomy, Uppsala University, Box 516, SE-75121, Uppsala, Sweden

[§]Helmholz-Zentrum Berlin, 12489 Berlin, Germany

Supporting Information

ABSTRACT: Silicon as a negative electrode material for lithium-ion batteries has attracted tremendous attention due to its high theoretical capacity, and fluoroethylene carbonate (FEC) was used as an electrolyte additive, which significantly improved the cyclability of silicon-based electrodes in this study. The decomposition of the FEC additive was investigated by synchrotron-based X-ray photoelectron spectroscopy (PES) giving a chemical composition depth-profile. The reduction products of FEC were found to mainly consist of LiF and $-\text{CHF}-\text{OCO}_2^-$ -type compounds. Moreover, FEC influenced the lithium hexafluorophosphate (LiPF_6) decomposition reaction and may have suppressed further salt degradation. The solid electrolyte interphase (SEI) formed from the decomposition of ethylene carbonate (EC) and diethyl carbonate (DEC), without the FEC additive present, covered surface voids and lead to an increase in polarization. However, in the presence of FEC, which degrades at a higher reduction potential than EC and DEC, instantaneously a conformal SEI was formed on the silicon electrode. This stable SEI layer sufficiently limited the emergence of large cracks and preserved the original surface morphology as well as suppressed the additional SEI formation from the other solvent. This study highlights the vital importance of how the chemical composition and morphology of the SEI influence battery performance.



INTRODUCTION

Silicon anode material is regarded as one of the most promising candidates for the next generation of lithium-ion batteries (LIBs) due to the substantially higher theoretical capacity (3578 mAh/g for $\text{Li}_{15}\text{Si}_4$) compared to that of conventional graphite (372 mAh/g for LiC_6).^{1,2} However, a severe problem related to its high gravimetric capacity is the huge volume change occurring during cycling (~300% volume expansion upon full lithiation), which consequently leads to high mechanical stress and breakdown of the conductive network of the composite electrode.^{3–5} As a result, the active material particles (Si) loose electrical contact with each other as well as with the conductive agent and the current collector, resulting in problems such as low Coulombic efficiency and poor capacity retention for silicon-based LIBs.^{6,7} Additionally, the solid electrolyte interphase (SEI) formed on the silicon surface is unstable and cannot sufficiently protect the electrode from further reaction with the electrolyte.⁷ Because of the formation of cracks, new SEI-free silicon surfaces are exposed to the electrolyte. This leads to a continuous SEI formation, which will consume the Li inventory and electrolyte solvent. The SEI generated on the silicon electrode with the conventional lithium hexafluorophosphate (LiPF_6) based electrolyte has been

studied and is found to mainly consist of LiF, lithium alkoxide, carbonate species such as lithium alkyl carbonates, Li_2CO_3 , and polycarbonate.^{8–11}

Several approaches have been explored in order to improve the silicon-based battery performance, for example, (i) control of the cycling voltage window to minimize volume change;¹² (ii) optimization of nanostructures to accommodate the volume change;^{13,14} (iii) distribution of the silicon particles in a matrix as Si/M (M, e.g., is carbon, graphene, etc.) nanocomposite material;^{15–17} (iv) use of binders with tailored functionalities;^{18–20} (v) use of better salts, e.g., LiFSI; and introduction of electrolyte additives, e.g., vinylene carbonate (VC), fluoroethylene carbonate (FEC), etc. to form a more stable SEI.^{21–24} Particularly, the FEC additive is found to substantially increase the Coulombic efficiency and enhance capacity retention.^{21–23} Various techniques have been applied to study the effect of the FEC additive. With transmission electron microscopy (TEM), a more uniform lithiation of silicon nanowires was observed when cycled with FEC-containing electrolyte compared to a

Received: January 27, 2015

Revised: March 9, 2015

Published: March 12, 2015



ACS Publications

© 2015 American Chemical Society

2591

DOI: 10.1021/acs.chemmater.5b00339
Chem. Mater. 2015, 27, 2591–2599

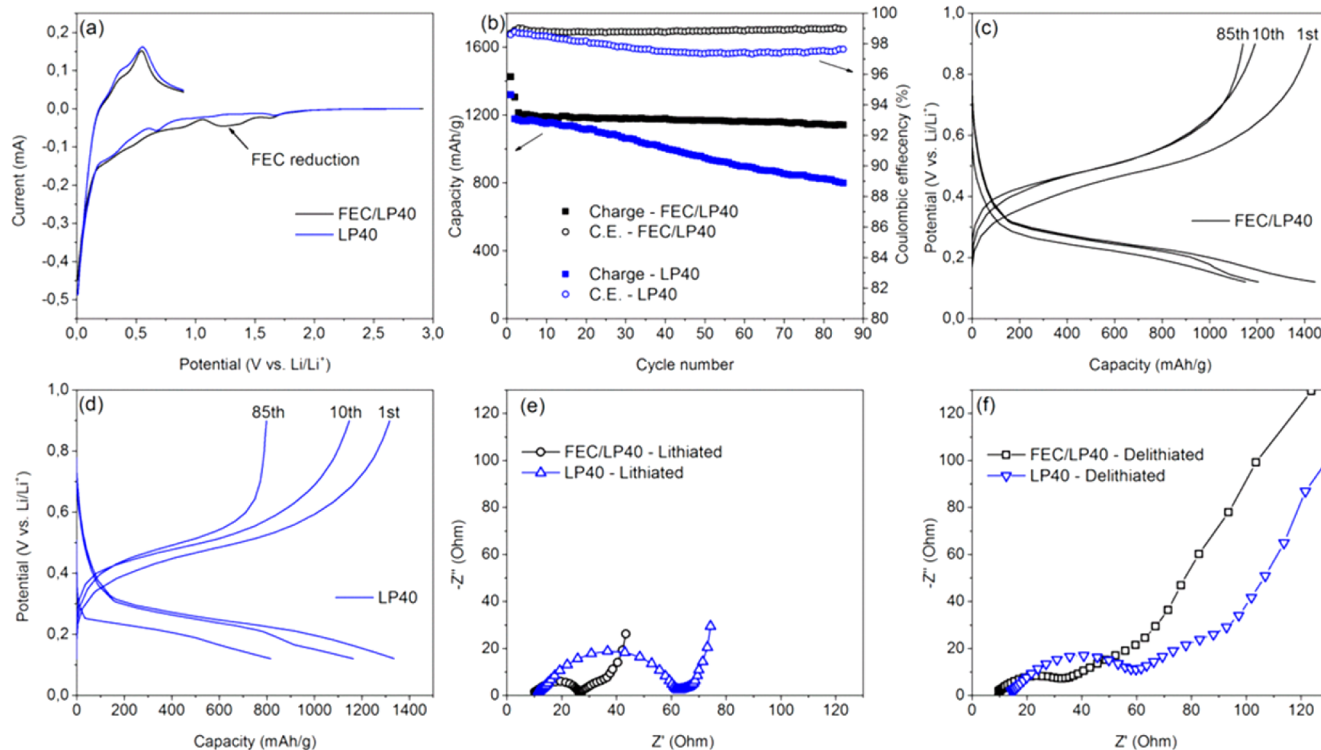


Figure 1. (a) Cyclic voltammetry results for the first cycle of silicon-based composite electrodes vs Li^0 half-cells with FEC/LP40 (black) and LP40 (blue) based electrolytes from OCV to 0.01 V and back to 0.9 V. (b) Gravimetric capacities and Coulombic efficiencies of the Si/ Li^0 half-cells cycled between 0.12 and 0.9 V at 500 mA/g (Si) using FEC/LP40 (black) and LP40 (blue) electrolytes. (c and d) Discharge and charge potential profile at 1st, 10th, and 85th cycles for FEC/LP40 (black) and LP40 (blue) cells, respectively. (e and f) EIS spectra for FEC/LP40 (black) and LP40 (blue) cells at a lithiated state (discharged to 0.12 V) and at a delithiated state (charged to 0.9 V), respectively.

nonuniform lithiation for a FEC-free system.²⁵ Electrochemical impedance spectroscopy (EIS) measurements confirmed that the overall impedance for FEC-containing silicon batteries was lower than that of FEC-free ones.^{25,26} Besides, Fourier transform infrared spectroscopy (FT-IR), nuclear magnetic resonance (NMR), and X-ray photoelectron spectroscopy (XPS) have been used in order to characterize the chemical composition of the SEI layer. LiF as the product of defluorination and polymerization products of the defluorinated FEC are suggested to be the main components, and these two routes are believed to be the main decomposition mechanisms of FEC.^{9,25,27} The ring opening reaction of FEC at the carbon–ether oxygen bond is also proposed as a possible pathway according to experimental and theoretical calculation results.^{21,28}

However, the mechanism of FEC decomposition and how the formed SEI layer influences electrochemical performance, so far, are still not fully understood, and more investigations are needed. Among all the characterization techniques used to investigate the SEI layers, photoelectron spectroscopy (PES) is a particularly powerful tool due to its surface sensitivity and the possibility to distinguish different chemical environments.²⁹ Moreover, synchrotron radiation based PES is capable of probing samples at different depths in a nondestructive way by varying the photon energy. In this context, the combination of synchrotron radiation based soft X-ray and hard X-ray PES was applied to investigate the SEI formation on the silicon electrodes cycled galvanostatically with or without the FEC additive. EIS and scanning electron microscopy (SEM) were also applied to aid the understanding of the electrochemical performance and morphology of the silicon anode.

EXPERIMENTAL SECTION

Battery Preparation. Silicon electrodes were prepared by coating a slurry of silicon nanopowder (average particle size \sim 50 nm, Alfa Aesar), super-P carbon black (Erachem Comilog), and sodium carboxymethyl cellulose (CMC-Na, DS = 0.9, Mw = 700000, Sigma-Aldrich) with a mass ratio of 80:12:8 onto copper foil. The slurry was prepared by 1 h of ball milling with a water–ethanol solution ($\text{H}_2\text{O}/\text{EtOH} = 7:3$) as solvent and cast on a Cu foil using doctor-blading. After predrying at 60 °C for 12 h, circular electrodes with a diameter of 20 mm were punched out and then further dried under vacuum at 120 °C for 12 h inside an argon-filled glovebox ($\text{O}_2 < 2 \text{ ppm}$, $\text{H}_2\text{O} < 1 \text{ ppm}$). The mass loading of silicon in the electrode coating was approximately 1.65 mg per punched electrode.

Two electrolytes were used for this study: (i) a pure commercialized LP40 (1 M LiPF_6 , ethylene carbonate (EC)/diethyl carbonate (DEC) = 1:1, Merck) and (ii) FEC/LP40 which consists of 90 wt % LP40 and 10 wt % FEC (99%, Aldrich). Silicon electrolyte/Li half-cells were assembled inside the argon-filled glovebox by sandwiching an electrolyte-soaked Solupor polymer separator between the two electrodes and vacuum-sealing into pouch-cells.

Electrochemical and Morphology Characterization. Cyclic voltammetry (CV) measurements for the first cycle were carried out on a MPG-2 potentiostat with a scan rate of 0.1 mV/s from open circuit voltage ($\text{OCV}, \sim 2.9 \text{ V vs Li/Li}^+$) to 0.01 and back to 0.9 V. The galvanostatic charge–discharge cycling of the assembled silicon half-cells were performed on a Digatron BTS-600 battery testing system at room temperature. For the cells’ discharge/charge stopped at selected potentials during the first cycle, the applied current was 150 mA/g of silicon ($\sim \text{C}/6$, corresponding to 1 mol of lithium in 6 h). For the longer cycling cells, a higher current, 500 mA/g of Si ($\sim \text{C}/2$, corresponding to 1 mol of lithium in 2 h), was used, and the cells were cycled between 0.12 and 0.9 V. In this case, precycling was performed prior to the regular galvanostatic cycling and consisted of four cycles where the batteries were discharged successively to 500, 1000, 1500,

and 2000 mAh/g of Si and charged up to 0.9 V. EIS measurements were performed on the batteries using an Autolab PGSTAT302N, and the frequency range used was 20 kHz to 10 mHz with a 10 mV amplitude perturbation. All electrochemical characterizations were performed at room temperature. The morphology of the samples was examined using scanning electron microscopy SEM/EDS Zeiss 1550 after being washed in dimethyl carbonate (DMC).

X-ray Photoelectron Spectroscopy. Before all XPS measurements, the batteries were disassembled inside an argon-filled glovebox, and the sample electrodes were carefully washed with DMC to reduce the amount of electrolyte residue. During washing, the electrodes were rinsed three times with 3 mL of DMC. The samples were transferred with a special-built airtight system directly from the glovebox to the spectrometer to avoid air exposure during the entire sample preparation and transfer processes.³⁰ All of the obtained XPS spectra were processed with Igor Pro 6 software and calibrated with a hydrocarbon C 1s signal at the binding energy of 285 eV after curve fitting.

In-House XPS. A PHI5500 spectrometer was used for in-house XPS measurements with monochromatized Al K α radiation ($\hbar\nu = 1486.7$ eV) as the excitation X-ray source. The quantification of relative surface atomic concentration was calculated as $C_x = (Ax/\sigma x)/\Sigma(Ay/\sigma y)$, where A is the integrated intensity of individual core level spectra, and σ is the sensitivity factor through the Multipak software (version 6.1A).

Soft X-ray PES. Soft X-ray PES measurements were performed at the Swedish national synchrotron radiation facility MAX IV Laboratory at the I411 beamline (Lund, Sweden), where the usable photon energy range is tunable from 50 to 1500 eV.³¹ X-rays were monochromatized by a Zeiss SX-700 plane grating monochromator, and the PES spectra were recorded with a Scienta R4000 WAL analyzer. For soft X-ray PES measurements, all PES core levels were measured with the same kinetic energy 140 eV for the photoelectrons in order to obtain the same probing depth, and this was achieved by varying the photon energy of the X-ray accordingly.

Hard X-ray PES. Hard X-ray PES characterizations were conducted at BESSY II synchrotron facility (HIKE end-station, KMC-1 beamline, Helmholtz Zentrum Berlin, Germany).^{32,33} Two different photon energies were used, 2005 and 6015 eV, corresponding to the first and third order X-ray from a Si(111) double-crystal monochromator. The PES spectra were recorded with a Scienta R4000 analyzer optimized for high kinetic energy up to 10 keV.

RESULTS AND DISCUSSION

Electrochemical Results. The electrochemical results are presented in Figure 1. CV measurements were performed on both FEC/LP40 and pure LP40 based electrolytes for the first electrochemical cycle. During discharge (reduction, lithiation), a reduction peak is visible at a potential of ~1.3 V (vs Li/Li $^+$) for the FEC/LP40 sample, while nothing is observed for the LP40 sample, indicating that this peak corresponds to the reduction of FEC.²⁷ The conventional SEI formation occurs at the potential of ~0.8 V (vs Li/Li $^+$), which is due to the decomposition of organic solvents such as EC, DEC, etc.^{34,35} With a higher reduction potential, FEC is reduced prior to the other solvents and thus quickly forms a surface layer, which consists of its degradation products as the initial SEI layer. Galvanostatic cycling for these two systems has also been performed, and the results for the first cycle are presented in Figure S1 (Supporting Information). With good similarity in voltage profile, the FEC/LP40 battery achieved slightly lower Coulombic efficiency (85.1% to 87.6%) compared to that of the LP40 battery. It can be related to more solvent reduction, especially due to the additional FEC in the electrolyte. In terms of long time cycling, the 10 wt % FEC substantially improved both the capacity retention and Coulombic efficiency as shown in Figure 1b. Only 5% capacity (referring to 1200 mAh/g) is

lost after 80 cycles with the FEC additive, whereas ~30% loss is observed without FEC. Meanwhile, the Coulombic efficiency is constantly retained at ~99% over the 85 cycles for the FEC/LP40 battery but continuously decreased to ~97% for the LP40 battery. Although with the precycling step, capacity loss can still be observed for both systems at the first few cycles after precycling for both FEC/LP40 and LP40 batteries. This capacity loss is attributed to the activation of silicon lithiation, and it can be seen as the change in discharge potential profile between the 1st and 10th cycle as shown in Figure 1c and d for the silicon half-cells cycled with or without FEC, respectively.³⁶ The polarization, especially the decrease in the lithiation potential, for the LP40 cell is found to be significantly larger than that for the FEC/LP40 cell after 85 cycles, and this results in lower capacity since constant potential cut-offs were used. As the polarization continuously increases, capacity fading will occur, which is observed here for the LP40 cell. Electrochemical impedance spectroscopy has been carried out to investigate this difference in polarization, and the results are shown in Figure 1e and f for the two systems both in lithiated and delithiated states. In general, the overall impedance is lower for the FEC/LP40 battery both in lithiated and delithiated states compared to that of the FEC-free one, and it is consistent with the finding from galvanostatic cycling results.

Surface Morphology: SEM. SEM images are presented in Figure 2 for a pristine Si electrode and the electrodes after 85

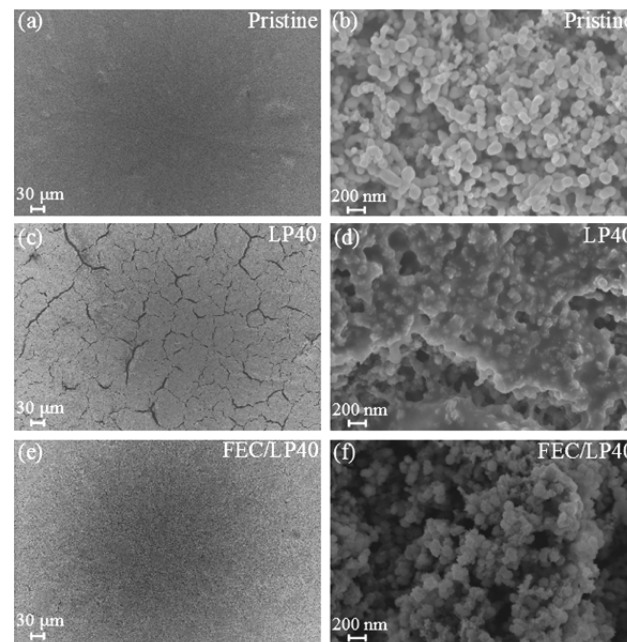


Figure 2. SEM images recorded with two different magnifications of the surface morphologies of pristine silicon electrodes (a,b) and after 85 cycles in the LP40 electrolyte (c,d) and in the FEC/LP40 electrolyte (e,f).

cycles with electrolyte LP40 (Figure 2c,d) and FEC/LP40 (Figure 2e,f). The Si nanoparticles, which have a typical size of ~50 nm in diameter, were homogeneously distributed in the pristine sample. However, after 85 cycles with electrolyte LP40, a large number of cracks with different sizes were formed on the electrode as seen in the low magnification images (Figure 2c). The surface of the silicon particles is found to be unevenly covered, most likely by the formed SEI layer. By adding 10 wt

% FEC into the LP40 electrolyte, the amount of cracks was significantly reduced as shown in Figure 1e. This can be one important reason for the lower impedance, which is observed for the cell cycled with the FEC/LP40 electrolyte. Moreover, with the reduced amount of cracks formed in this case, less fresh electrode surface is exposed to form an extra SEI layer, and a higher Coulombic efficiency is obtained. Another interesting difference that can be observed here between the two electrodes is that the morphology is completely different in the high magnification images. An increase in particle size was observed for the FEC/LP40 sample, indicating the formation of SEI. Compared to the LP40 sample, this formed SEI appears more homogeneous, and the original morphology of the pristine sample was much better preserved after long-term cycling in the FEC/LP40 case. As a result, the uniform SEI layer on the FEC/LP40 sample kept the silicon particles in good contact with the electrolyte, which limits the increase in impedance.

Besides, larger polarization for the lithiation process compared to delithiation can be observed in the electrochemical results (Figure 1c and d) for both the FEC/LP40 and LP40 samples. Similar results were obtained by Oumellal et al., and it was suggested that this was attributed to kinetic restriction since the diffusion of Li^+ through the composite electrode was limited.⁷ According to the SEM images, the electrode surface voids were substantially covered by the SEI for the LP40 sample so that the access of liquid electrolyte was thus more limited compared to that of the FEC/LP40 sample where the overall morphology was well preserved, similar to the pristine electrode. This can be another reason for the larger polarization for the LP40 sample and faster capacity decay.³⁷ Overall, these results prove that the morphology of the SEI layer can be essential for the battery performance and substantially influenced by the use of FEC.

PES Characterization. SEI formation on silicon electrodes with FEC/LP40 as the electrolyte at different states of charge (SOCs) (highlighted as black dots in Figure 3) during the first electrochemical cycle was investigated by PES. In addition, the cell cycled for 85 cycles was also studied to evaluate SEI evolution after long cycling. Cells after 1 and 85 cycles without the FEC additive will be compared in this study to give a better

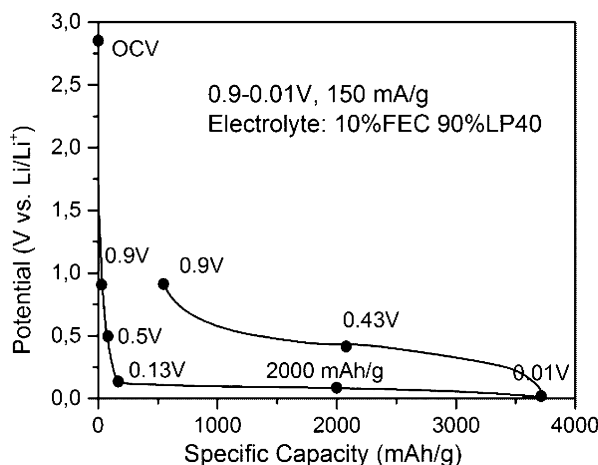


Figure 3. First electrochemical cycle of the silicon-based electrode vs Li^+ half-cells using the FEC/LP40 electrolyte. The samples at specific SOC (highlighted with black dots in the figure) have been characterized by PES.

understanding of the role of FEC as an effective electrolyte additive.

Depth-profiling was performed by varying the X-ray photon energy at two synchrotron facilities, and all of the samples have been measured at three different depths as presented in Table S1 (Supporting Information). Different photon energies were chosen for each core level when performing soft X-ray PES in order to obtain the same kinetic energy of photoelectrons, i.e., the same probing depth. The electron inelastic mean free path (IMFP) is extremely sensitive to the kinetic energy of photoelectrons for soft X-ray PES, and by using the same kinetic energy, all different core levels can be probed at the same depth. The kinetic energy selected here is 140 eV, which gives a probing depth of $\sim 2 \text{ nm}$.^{35,38,39} For the hard X-ray PES measurements, two photon energies, 2005 and 6015 eV, were used, which correspond to probing depths of $\sim 14 \text{ nm}$ and $\sim 40 \text{ nm}$, respectively.

Initial SEI Formation: The Decomposition of FEC (OCV to 0.13 V (vs Li/Li^+)). The most surface sensitive measurements (soft X-ray PES) were performed on a soaked sample (referred to as the OCV sample) and on samples discharged to 0.9 V, 0.5 V, 0.13 V vs Li/Li^+ . As described in the Experimental Section, measurements were carried out with the same kinetic energy, 140 eV, which gives the same probing depth of $\sim 2 \text{ nm}$, i.e., different photon energies were used depending on the core level recorded. The evolution of the F 1s, O 1s, and C 1s spectra is shown in Figure 4. For the OCV sample, all F 1s, O 1s, and C 1s spectra are dominated by the contribution from species of LiPF_6 , SiO_x , carbon black, and CMC-Na. No traces of FEC are observed, indicating successful removal of the FEC residue through washing with DMC on the OCV sample. As shown in the CV results (Figure 1a) where the reduction of FEC occurs at the potential of $\sim 1.3 \text{ V}$ (vs Li/Li^+), the signal of its decomposition products becomes visible for the 0.9 V sample, especially in the F 1s and C 1s spectra. LiF (F 1s peak at 685 eV), which is a common SEI component in F-containing battery systems, is formed and observed in the F 1s spectra as expected when the battery was discharged to 0.9 V. LiF can be formed from the defluorination of FEC as well as the degradation of LiPF_6 via chemical decomposition and subsequent hydrolysis.⁴⁰ Besides the contribution of the salt LiPF_6 residue at 687.5 eV to the F 1s spectrum, another fluorinated species is observed with a binding energy of $\sim 686.3 \text{ eV}$, which corresponds to a F-C environment.⁴¹ This is confirmed by the increase in intensity of the C 1s peak at $\sim 288 \text{ eV}$ when the electrode is discharged to 0.9 V (vs Li/Li^+). The peak position is attributed to monofluorinated carbon, which is mostly attributed to the decomposition product of FEC. The slightly decreased carbon black signal indicates that a thin layer of SEI has been formed once the battery is discharged to 0.9 V. Besides, another new C 1s feature at $\sim 290.8 \text{ eV}$ (red filling in Figure 1) can be observed for the 0.9 V. The binding energy is slightly higher than the C 1s signal of conventional carbonate species, which are usually located at $\sim 290 \text{ eV}$.^{41–43} This signal is attributed to the carbonate group ($-\text{CHF}-\text{OCO}_2$ -type) resulting from the FEC decomposition, which is influenced by the $-\text{CHF}-$ group. Most likely, this type of compound is formed via a ring opening reaction of FEC. However, it is difficult to pinpoint exactly which bond breaks during ring opening using only PES techniques. Although the ring opening decomposition mechanism has been proposed in the literature,^{21,28} in this study, different products ($-\text{CHF}-\text{OCO}_2$ -type) are identified with high-resolution PES. Detailed FEC decomposition

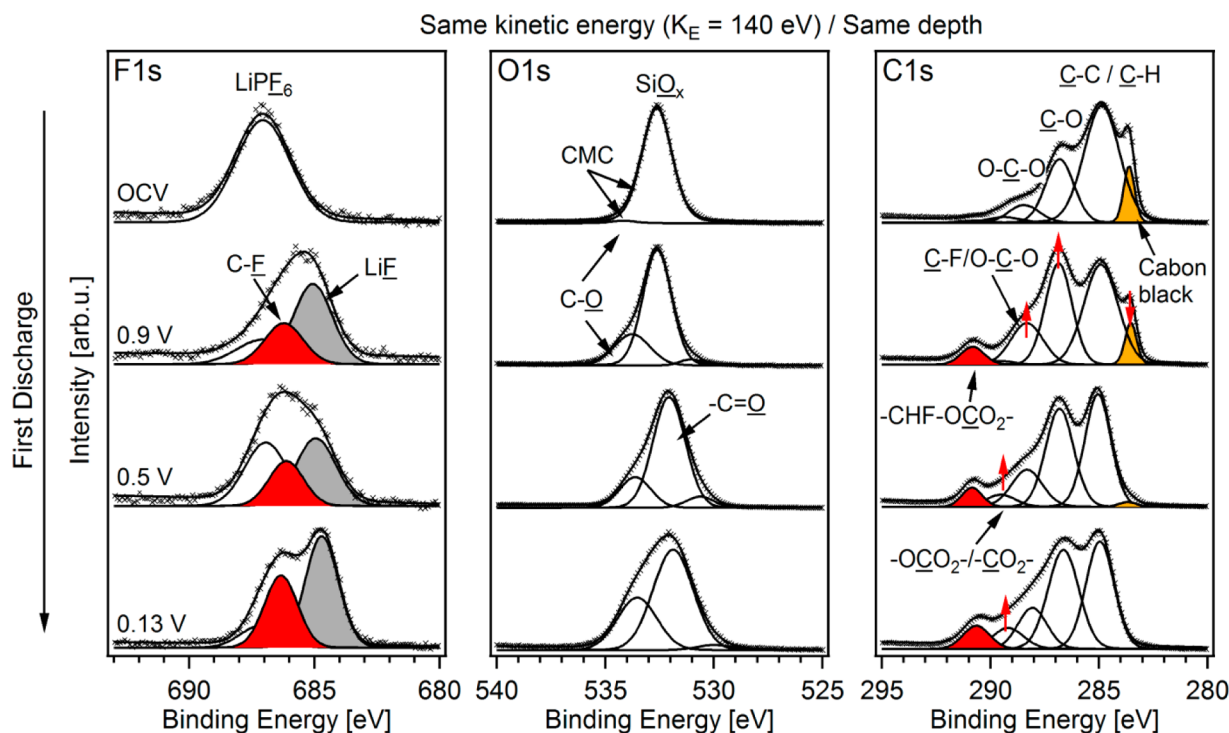
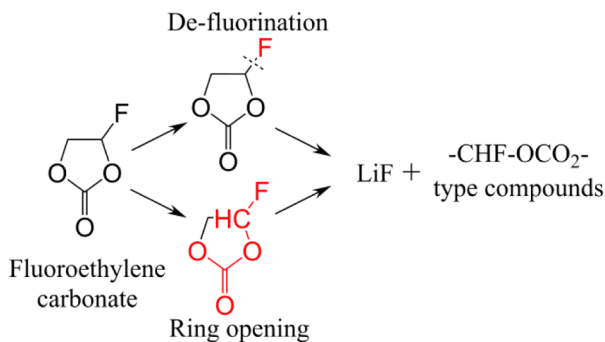


Figure 4. F 1s, O 1s, and C 1s spectra of the silicon electrode at different SOC (OCV, 0.9 V, 0.5 V, and 0.13 V vs Li/Li⁺ from top to bottom). The electrolyte used here was FEC/LP40, and the kinetic energy of the core level photoelectrons was kept the same, 140 eV, to obtain the same probing-depth for all elements.

mechanisms suggested by our PES results are presented in Scheme 1.

Scheme 1. Possible FEC Decomposition Reactions and Products



When the Si electrode is further discharged to 0.5 and 0.13 V, the thickness of the SEI layer continues to grow; thus, the intensity of the carbon black peak decreases and is no longer detected at 0.13 V vs Li/Li⁺. It indicates that at this stage, the SEI layer is thicker than the probing depth, i.e., 2 nm. For 0.5 and 0.13 V samples, the main O 1s peak is located at ~532 eV, and it is attributed to carbonyl oxygen. This feature is coincident with the increase in intensity of the carbonate/carboxylate carbon peak (at ~289.4 eV) in C 1s for the 0.5 and 0.13 V sample. More of the SEI species were formed between 0.5 and 0.13 V according to the indepth analysis results shown in Figure S2 (Supporting Information). There is no dramatic change in C 1s spectra until the battery was discharged to 0.13 V where the intensity of the carbon black peak has substantially decreased compared to that of the other C-species. However,

the SEI layer formed until this SOC is still limited to a few nanometers in thickness since the carbon black signal is still relatively strong and visible in the 2005 eV measurement shown in Figure S2 (Supporting Information), which has a probing depth of 14 nm. After the initial SEI formation, the SEI layer on FEC/LP40 samples is found to consist of LiF, -CHF-OCO₂-type of compounds, carbonate/carboxylate, and ether-type species.

SEI Evolution during the First Lithiation and Delithiation. To investigate the SEI evolution during the first lithiation (from 0.13 to 0.01 V) and first delithiation (from 0.01 to 0.9 V), PES measurements with higher photon energy, i.e., deeper probing depth, were performed using hard X-ray PES. Two different photon energies, 2005 and 6015 eV, were used for the samples at SOCs of 0.13, 0.01, and 0.9 V, and the results are presented in Figure 5.

In general, the composition of the SEI layer is found to be rather consistent during the first cycle after the initial SEI formation since no significant peak shift or appearance of new peaks is visible in the C 1s spectra in Figure 5. However, the thickness of the SEI layer has increased considerably during the first lithiation since the carbon black (CB) peak is no longer visible in the 2005 eV result and has rather low intensity even in the more bulk-sensitive (6015 eV) measurement. This means that the thickness of the SEI layer has reached at least 15 nm. However, carbon black becomes more pronounced at the 0.9 V sample, which has been fully delithiated. One reason can be the formation of cracks, which will expose the fresh electrode surface. Another reason is the dissolution of SEI components during the first delithiation process. Previous studies on the SEI evolution on graphite suggested that the formation of the SEI layer is a dynamic process and that the thickness of the SEI layer is reduced during delithiation for anode materials.^{38,44} This means that the SEI components are chemically or

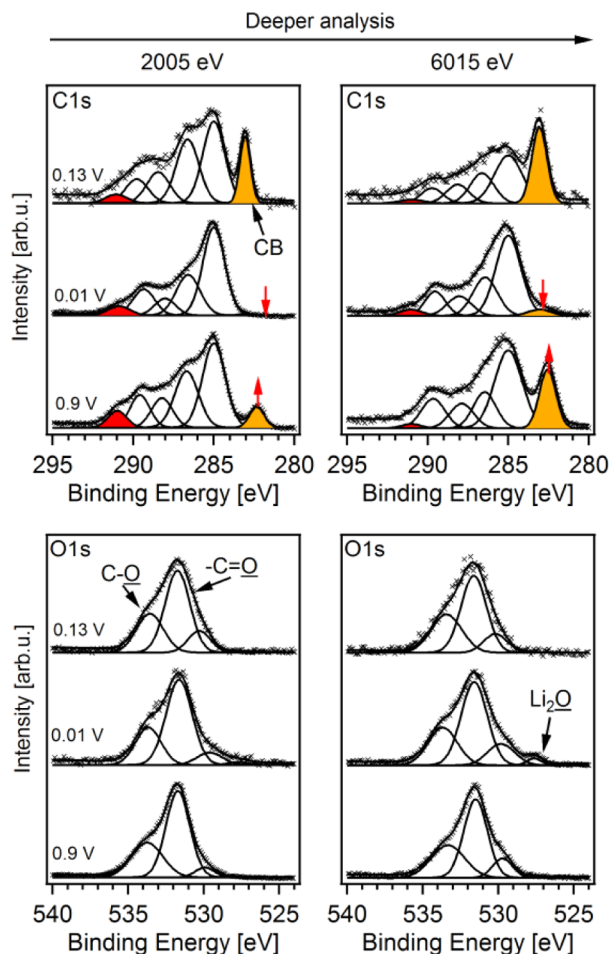


Figure 5. C 1s and O 1s spectra of the Si-based electrode just before lithiation (0.13 V vs Li/Li⁺), at the end of the discharge (0.01 V vs Li/Li⁺) and at the end of the charge (0.9 V vs Li/Li⁺). The photon energies were 2005 and 6015 eV, and the electrolyte applied to these samples was FEC/LP40.

electrochemically decomposed and removed, which could be the same reason for our observation here.

There is only one new compound detected after the first lithiation, and it has an O 1s signal at ~528 eV, which is attributed to Li₂O. It is quite clear that it formed after lithiation and disappeared after delithiation. Besides, it can only be detected by higher photon energy (6015 eV), suggesting that it is buried underneath the SEI layer. This formation of Li₂O could be attributed to the reduction of the thin SiO_x layer, which can be identified by extreme surface sensitive PES measurements (shown in Figure S3, Supporting Information).⁸

SEI Evolution after Long Cycling (85 Cycles) and Salt Decomposition. The evolution of the SEI layer formed on silicon electrodes which have been cycled with or without FEC additive is compared in this section. Figure 6 presents the overview and F 1s spectra which are measured with $h\nu$ of 2005 eV for the silicon electrodes cycled with FEC/LP40 and LP40 after 85 cycles, respectively. Atomic concentration quantification was done with in-house XPS measurements on the silicon electrodes for these two systems, and the results are shown in Table 1. A significant difference in elemental composition can be observed between the two kinds of batteries. The FEC generates more fluorinated species, which correspond to LiF, FEC-decomposition products (C–F compounds), and salt

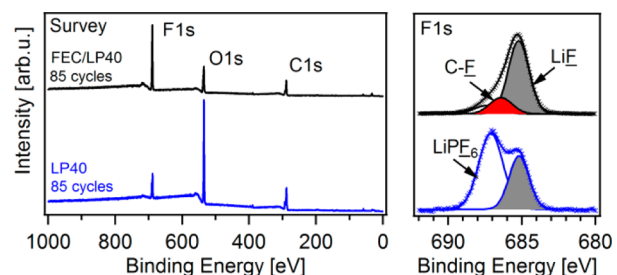


Figure 6. Overview and F 1s spectra of the silicon electrodes after 85 cycles with electrolytes FEC/LP40 (black) and LP40 (blue), respectively. The photon energy used for these measurements was 2005 eV.

Table 1. Surface Atomic Percentage of Silicon Electrodes after 85 Cycles with FEC/LP40 and LP40 Electrolytes^a

electrolyte	F 1s (%)	O 1s (%)	C 1s (%)	P 2p (%)	Si 2p (%)	Li 1s (%)
FEC/LP40	15.7	26.4	36.6	0.5	0.3	20.5
LP40	4.1	31.9	48.7	0.9	0.4	14.0

^aThe measurements were carried out with in-house XPS (photon energy of 1486.7 eV).

residues. Since the only difference between these two systems is the additional 10 wt % FEC in the electrolyte, FEC should be the source of the additional amount of LiF. Previously, Lu et al. proved that LiF significantly enhanced the cyclability of Li₄Ti₅O₁₂ anode, and the simulation results from Ganesh et al. also showed the importance of inorganic species such as LiF and Li₂CO₃.^{45,46} The majority of the SEI on the electrode which was cycled with pure LP40 is oxygen-containing species, e.g., carbonate species. Moreover, the F-containing species are homogeneously distributed across the SEI, supported by the depth probing of F 1s, which shows no difference between the results from two probing depth (shown in Figure S4, Supporting Information).

The C 1s spectra measured with photon energies of 430, 2005, and 6015 eV for FEC/LP40 and LP40 batteries after 1 and 85 cycles are presented in Figure 7 in black and blue, respectively. For both FEC/LP40 samples, the peaks at ~290.8 eV (red in Figure 7) corresponding to decomposition product of FEC can be observed in all three depth results. However, none of the results from the LP40 sample has the presence of such a peak. The signal with highest binding energy is at 290 eV, which is commonly attributed to conventional carbonate species produced from the degradation of solvent EC/DEC. This confirms that the C 1s peak at 290.8 eV is unique for the FEC/LP40 battery and that it corresponds to the degradation product (–CHF–OCO₂-type) of FEC. Interestingly, besides the unique C–F peak, the C 1s signals which correspond to O–C–O and –OCO₂– compounds in the FEC/LP40 case are slightly shifted from the ones in the LP40 case. This indicates that these compounds are in different chemical composition and that most likely it is because of the degraded FEC segments taking part in the formation of different compounds compared to just LP40 batteries. The thickness of the SEI layer has been widely discussed and considered as an essential parameter on how the SEI influences battery performance.^{29,43,47,48} Unfortunately, it is not valid here to estimate SEI thickness within the PES results since the estimation will only be valid when the SEI layer is homogeneously distributed on the electrode. As the SEM images show in Figure 2, the SEI layer formed on the

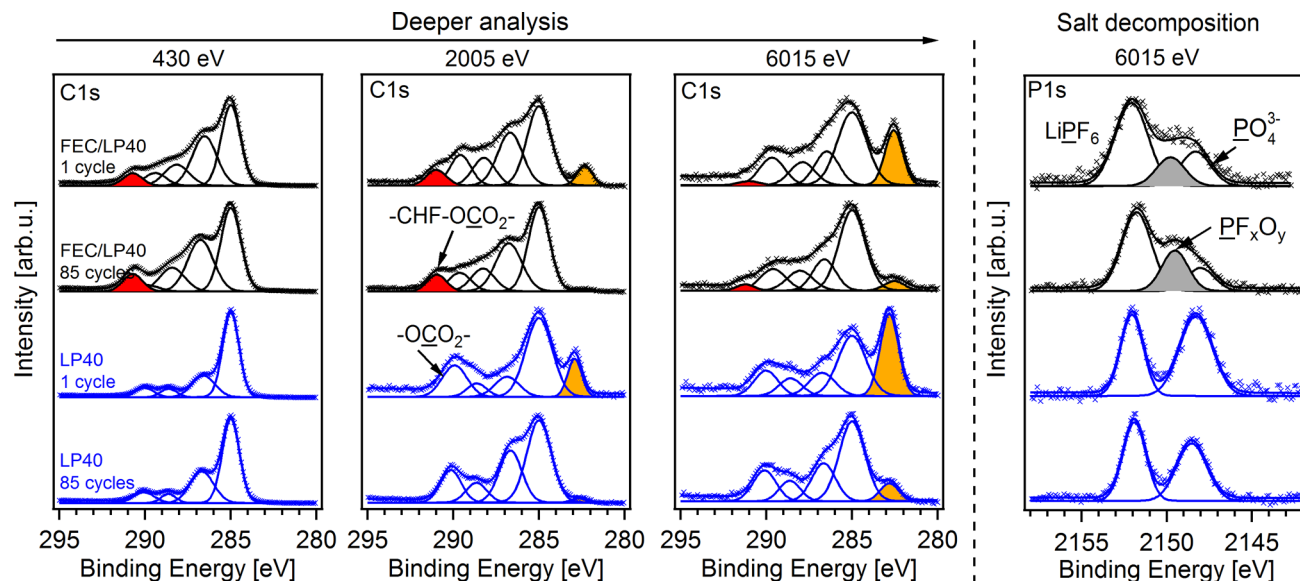


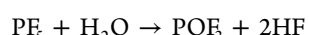
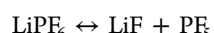
Figure 7. C 1s and P 1s spectra of the silicon electrodes at 3 different probing depths after 1 and 85 cycles with electrolyte FEC/LP40 (black) and LP40 (blue), respectively. Three different excitation energies 430, 2005, and 6015 eV were used.

silicon electrode cycled with the LP40 electrolyte is unevenly covering the electrode. However, instead of the thickness of the SEI layer, its chemical composition and homogeneity of the coverage seem to play a more important role in influencing battery performance according to our observations. The SEI formed on the electrode, which was cycled with the FEC/LP40 electrolyte, consists of more inorganic species like LiF as well as organic species but in different composition. Moreover, from the high magnification SEM images, this SEI uniformly covers silicon particles and preserves the surface voids even after 85 cycles. It is proved that this can sufficiently limit continuous SEI formation from decomposition of other organic solvent and achieve excellent capacity retention and high Coulombic efficiency. On the contrary, the SEI formed on the LP40 cycled electrode severely damaged the surface void structure, which can lead to a dramatic increase in impedance and rapid capacity decay.

Although it is not ideal to estimate SEI thickness with XPS results here, particularly when comparing different systems which have significant difference in morphologies, non-destructive depth-profiling PES characterizations still can provide valuable information on the evolution of the SEI layer within one system. Moreover, the knowledge of the chemical composition and its depth-distribution for a SEI layer obtained from PES can be very helpful in understanding its formation mechanism and functionality.

Besides the C 1s results, O 1s spectra have also been analyzed and presented in Figure S5 (Supporting Information). The results show good consistency in composition after cycling for both FEC/LP40 and LP40-only batteries. For the FEC/LP40 silicon electrode, the O 1s has ether-oxygen (\sim 533.5 eV) and carbonyl oxygen (\sim 532 eV) in similar amounts. However, for the FEC-free silicon electrode, the O 1s is dominated by a carbonyl oxygen signal at \sim 532 eV. That would be attributed to the carbonate and carboxylate species formed from the reduction of organic solvent in the electrolyte. Unlike the SEI on the FEC/LP40 sample, which has rather evenly distributed O-species, the inner part of the SEI formed on the LP40 sample contains more carbonate species since its signal becomes more dominating in higher $h\nu$ measurements.

Since P 2p overlaps with silicon plasmonic signals, it will not be possible to use the obtained spectra for further analysis. Thus, we hereby present P 1s spectra as shown in Figure 7 for FEC/LP40 and LP40 samples after 1 and 85 cycles, respectively. The photon energy used for the measurements was 6015 eV. Two signals dominate the P 1s spectra for both LP40 based batteries after 1 cycle and 85 cycles. These two peaks correspond to the LiPF₆ residue at \sim 2152 eV and phosphate compounds at \sim 2148.3 eV, which is a rather normal LiPF₆ decomposition product found on LiPF₆-based electrolyte batteries.^{30,38,43,44} Besides these two compounds, another distinct signal at \sim 2149.6 eV can be observed for both 1 cycle and 85 cycle LP40/FEC batteries. Although there is a lack of reference for the P 1s core level, the oxidation state of this phosphorus signal can be assigned to +5 since the oxidation states for the other two peaks are both +5. This species has higher binding energy than phosphates, and therefore, it would most likely to be fluorinated. Since the only phosphorus source in the battery is the LiPF₆ salt, this new species indicates the formation of another degradation product of LiPF₆. The degradation mechanism for LiPF₆ is suggested to be⁴⁰



In the presence of higher fluorinated phosphoric oxides, it is most likely that the decomposition reaction of the salt is suppressed in the battery which has the FEC additive in the electrolyte. This can be one additional key point explaining why FEC could substantially increase the performance of the silicon electrode as well as other electrode materials. The suppression of the salt degradation is probably due to the decomposed FEC segments, which may interact with the salt and form a stable intermediate decomposition product. Moreover, the initially formed SEI layer from the decomposition of FEC may also help reduce further degradation of LiPF₆.

CONCLUSIONS

The influence of the effective electrolyte additive FEC has been investigated by comparing the electrochemical performance,

morphology, and SEI formation between silicon half-cells cycled with or without this additive. Significant improvement in capacity retention and Coulombic efficiency was obtained by adding 10 wt % FEC into the commercial LP40 electrolyte. The morphology study by SEM shows that much less cracks were formed on the silicon electrode cycled with the FEC/LP40 electrolyte. Moreover, the conformal SEI layer on the FEC/LP40 cycled silicon electrode covered silicon particles more homogeneously and better preserved the surface voids than the LP40 cycled electrode. Both of these two differences can lead to a lower polarization and thus lower total impedance for the FEC/LP40 battery. Schematic drawings of the SEI formation on silicon electrodes after long-term cycling with FEC/LP40 (Figure 8a) and LP40 (Figure 8b) electrolytes, respectively, are presented in Figure 8.

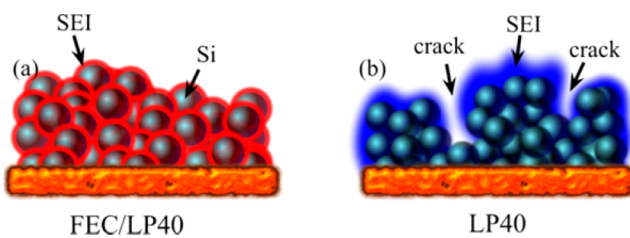


Figure 8. Schematic representation of SEI formation on a silicon anode which is long-time cycled with different electrolytes FEC/LP40 (a) and LP40 (b). The two SEI layers are different in composition and are highlighted with different colors.

Synchrotron radiation based X-ray photoelectron spectroscopy with various photon energies for depth profiling was applied to investigate the decomposition of FEC and the composition difference between the SEI layers formed with and without the FEC additive. Without the presence of FEC, the SEI layer is dominated by carbon and oxygen containing species, which are mainly EC/DEC degradation products. With a higher reduction potential, FEC degrades prior to EC/DEC and forms an initial SEI, which consists of larger amounts of LiF together with other organic species ($-\text{CHF}-\text{OCO}_2$ -type compounds). These compounds are homogeneously distributed across the SEI according to depth profiling. This SEI covers silicon particles evenly and is mechanically strong enough to prevent the formation of large amounts of cracks. Moreover, the initially formed SEI can substantially limit the degradation of EC/DEC and thus prevent the continuous development of an inhomogeneous SEI layer. According to the high resolution PES results, defluorination and ring-opening are found to be the two most possible degradation routes for FEC on silicon electrodes. The FEC additive is also found to be able to influence the LiPF_6 decomposition reaction, and this could be due to the formation of a stable SEI from the decomposition of FEC or the formation of stable intermediate degradation products with FEC decomposition segments. This study shows the importance not only of the SEI thickness but also of the chemical composition and the morphology of the SEI in influencing electrochemical behavior. We believe that this study could pave the way to systematically understand the solid electrolyte interphase.

■ ASSOCIATED CONTENT

Supporting Information

Potential profile for FEC/LP40 and LP40 silicon half-cells during the first cycle; the excitation conditions for different PES measurements and estimated probing depths; C 1s spectra of the silicon electrodes at different states of charge (OCV, 0.9, 0.5, and 0.13 V) measured with photon energies of 2005 eV and 6015 eV; Si 2p spectrum of the pristine Si electrode; F 1s spectra of the silicon electrodes after 1 and 85 cycles with electrolyte FEC/LP40 measured with photon energies of 2005 and 6015 eV; and O 1s spectra of the silicon electrodes after 1 and 85 cycles with electrolytes FEC/LP40 and LP40, respectively. This material is available free of charge via the Internet at <http://pubs.acs.org>.

■ AUTHOR INFORMATION

Corresponding Author

*E-mail: tobjorn.gustafsson@kemi.uu.se.

Notes

The authors declare no competing financial interest.

■ ACKNOWLEDGMENTS

We acknowledge Chenjuan Liu for assistance with SEM experiments and Julia Maibach for helpful discussions. The research leading to these results has received funding from the Swedish Energy Agency under grant agreement 34191-1, the Swedish Governmental Agency for Innovation Systems (Vinnova), and the European Community's Seventh Framework Programme (FP7/2007-2013) under grant agreement No. 312284. We also thank Helmholtz-Zentrum Berlin for the allocation of synchrotron radiation beamtime and providing financial support for travel.

■ REFERENCES

- (1) Obrovac, M. N.; Christensen, L. *Electrochem. Solid-State Lett.* **2004**, *7*, A93.
- (2) Etacheri, V.; Marom, R.; Elazari, R.; Salitra, G.; Aurbach, D. *Energy Environ. Sci.* **2011**, *4*, 3243.
- (3) Benedek, R.; Thackeray, M. M. *J. Power Sources* **2002**, *110*, 406.
- (4) Chon, M. J.; Sethuraman, V. A.; McCormick, A.; Srinivasan, V.; Guduru, P. R. *Phys. Rev. Lett.* **2011**, *107*, 45503.
- (5) Zhang, L. Q.; Liu, X. H.; Liu, Y.; Huang, S.; Zhu, T.; Gui, L.; Mao, S. X.; Ye, Z. Z.; Wang, C. M.; Sullivan, J. P.; Huang, J. Y. *ACS Nano* **2011**, *5*, 4800.
- (6) Ryu, J. H.; Kim, J. W.; Sung, Y.-E.; Oh, S. M. *Electrochem. Solid-State Lett.* **2004**, *7*, A306.
- (7) Oumella, Y.; Delpuech, N.; Mazouzi, D.; Dupré, N.; Gaubicher, J.; Moreau, P.; Soudan, P.; Lestriez, B.; Guyomard, D. *J. Mater. Chem.* **2011**, *21*, 6201.
- (8) Philippe, B.; Dedryvère, R.; Gorgoi, M.; Rensmo, H.; Gonbeau, D.; Edström, K. *Chem. Mater.* **2013**, *25*, 394.
- (9) Nie, M.; Abraham, D. P.; Chen, Y.; Bose, A.; Lucht, B. L. *J. Phys. Chem. C* **2013**, *117*, 13403.
- (10) Chan, C. K.; Ruffo, R.; Hong, S. S.; Cui, Y. *J. Power Sources* **2009**, *189*, 1132.
- (11) Nadimpalli, S. P. V.; Sethuraman, V. A.; Dalavi, S.; Lucht, B.; Chon, M. J.; Shenoy, V. B.; Guduru, P. R. *J. Power Sources* **2012**, *215*, 145.
- (12) Obrovac, M. N.; Krause, L. *J. Electrochem. Soc.* **2007**, *154*, A103.
- (13) Chan, C. K.; Peng, H.; Liu, G.; McIlwrath, K.; Zhang, X. F.; Huggins, R. A.; Cui, Y. *Nat. Nanotechnol.* **2008**, *3*, 31.
- (14) Wu, H.; Cui, Y. *Nano Today* **2012**, *7*, 414.
- (15) Lee, J. K.; Smith, K. B.; Hayner, C. M.; Kung, H. H. *Chem. Commun. (Cambridge, U. K.)* **2010**, *46*, 2025.

- (16) Ren, J.-G.; Wu, Q.-H.; Hong, G.; Zhang, W.-J.; Wu, H.; Amine, K.; Yang, J.; Lee, S.-T. *Energy Technol.* **2013**, *1*, 77.
- (17) Zhang, R.; Du, Y.; Li, D.; Shen, D.; Yang, J.; Guo, Z.; Liu, H. K.; Elzatahry, A. A.; Zhao, D. *Adv. Mater.* **2014**, *26*, 6749.
- (18) Wang, C.; Wu, H.; Chen, Z.; McDowell, M. T.; Cui, Y.; Bao, Z. *Nat. Chem.* **2013**, *5*, 1042.
- (19) Wu, M.; Xiao, X.; Vukmirovic, N.; Xun, S.; Das, P. K.; Song, X.; Olalde-Velasco, P.; Wang, D.; Weber, A. Z.; Wang, L. W.; Battaglia, V. S.; Yang, W.; Liu, G. *J. Am. Chem. Soc.* **2013**, *135*, 12048.
- (20) Jeena, M. T.; Lee, J. I.; Kim, S. H.; Kim, C.; Kim, J. Y.; Park, S.; Ryu, J. H. *ACS Appl. Mater. Interfaces* **2014**, *6*, 18001.
- (21) Nakai, H.; Kubota, T.; Kita, A.; Kawashima, A. *J. Electrochem. Soc.* **2011**, *158*, A798.
- (22) Dalavi, S.; Guduru, P.; Lucht, B. L. *J. Electrochem. Soc.* **2012**, *159*, A642.
- (23) Lin, Y.-M.; Klavetter, K. C.; Abel, P. R.; Davy, N. C.; Snider, J. L.; Heller, A.; Mullins, C. B. *Chem. Commun. (Cambridge, U.K.)* **2012**, *48*, 7268.
- (24) Philippe, B.; Dedryvère, R.; Gorgoi, M.; Rensmo, H.; Gonbeau, D.; Edström, K. *J. Am. Chem. Soc.* **2013**, *135*, 9829.
- (25) Etacheri, V.; Haik, O.; Goffer, Y.; Roberts, G. a.; Stefan, I. C.; Fasching, R.; Aurbach, D. *Langmuir* **2012**, *28*, 965.
- (26) Bordes, A.; Eom, K.; Fuller, T. F. *J. Power Sources* **2014**, *257*, 163.
- (27) Profatilova, I. A.; Stock, C.; Schmitz, A.; Passerini, S.; Winter, M. *J. Power Sources* **2013**, *222*, 140.
- (28) Leung, K.; Rempe, S. B.; Foster, M. E.; Ma, Y.; Martinez del la Hoz, J. M.; Sai, N.; Balbuena, P. B. *J. Electrochem. Soc.* **2013**, *161*, A213.
- (29) Verma, P.; Maire, P.; Novák, P. *Electrochim. Acta* **2010**, *55*, 6332.
- (30) Malmgren, S.; Ciosek, K.; Lindblad, R.; Plogmaker, S.; Kühn, J.; Rensmo, H.; Edström, K.; Hahlin, M. *Electrochim. Acta* **2013**, *105*, 83.
- (31) Bässler, M.; Ausmees, A.; Jurvansuu, M.; Feifel, R.; Forsell, J. O.; de Tarso Fonseca, P.; Kivimäki, A.; Sundin, S.; Sorensen, S. L.; Nyholm, R.; Björneholm, O.; Aksela, S.; Svensson, S. *Nucl. Instrum. Methods Phys. Res., Sect. A* **2001**, *469*, 382.
- (32) Schaefers, F.; Mertin, M.; Gorgoi, M. *Rev. Sci. Instrum.* **2007**, *78*, 123102.
- (33) Gorgoi, M.; Svensson, S.; Schäfers, F.; Öhrwall, G.; Mertin, M.; Bressler, P.; Karis, O.; Siegbahn, H.; Sandell, A.; Rensmo, H.; Doherty, W.; Jung, C.; Braun, W.; Eberhardt, W. *Nucl. Instrum. Methods Phys. Res., Sect. A* **2009**, *601*, 48.
- (34) Fong, R.; von Sacken, U.; Dahn, J. R. *J. Electrochem. Soc.* **1990**, *137*, 2009.
- (35) Philippe, B.; Dedryvère, R.; Allouche, J.; Lindgren, F.; Gorgoi, M.; Rensmo, H.; Gonbeau, D.; Edström, K. *Chem. Mater.* **2012**, *24*, 1107.
- (36) Nguyen, B. P. N.; Chazelle, S.; Cerbelaud, M.; Porcher, W.; Lestriez, B. *J. Power Sources* **2014**, *262*, 112.
- (37) Radvanyi, E.; Porcher, W.; De Vito, E.; Montani, A.; Franger, S.; Jouanneau Si Larbi, S. *Phys. Chem. Chem. Phys.* **2014**, *16*, 17142.
- (38) Ciosek Höglström, K.; Malmgren, S.; Hahlin, M.; Rensmo, H.; Thébault, F.; Johansson, P.; Edström, K. *J. Phys. Chem. C* **2013**, *117*, 23476.
- (39) Painter, L. R.; Arakawa, E. T.; Williams, M. W.; Ashley, J. C. *Radiat. Res.* **1980**, *83*, 1.
- (40) Aurbach, D.; Markovsky, B.; Shechter, A.; Ein-Eli, Y.; Cohen, H. *J. Electrochem. Soc.* **1996**, *143*, 3809.
- (41) Beamson, G.; Briggs, D. *High Resolution XPS of Organic Polymers: The Scienta ESCA300 Database*; John Wiley & Son Ltd.: West Sussex, England, 1992.
- (42) Younesi, R.; Hahlin, M.; Björefors, F.; Johansson, P.; Edström, K. *Chem. Mater.* **2013**, *25*, 77.
- (43) Malmgren, S.; Ciosek, K.; Hahlin, M.; Gustafsson, T.; Gorgoi, M.; Rensmo, H.; Edström, K. *Electrochim. Acta* **2013**, *97*, 23.
- (44) Ciosek Höglström, K.; Malmgren, S.; Hahlin, M.; Gorgoi, M.; Nyholm, L.; Rensmo, H.; Edström, K. *Electrochim. Acta* **2014**, *138*, 430.
- (45) Lu, Y.; Tu, Z.; Archer, L. A. *Nat. Mater.* **2014**, *13*, 961.
- (46) Ganesh, P.; Kent, P. R. C.; Jiang, D.-E. *J. Phys. Chem. C* **2012**, *116*, 24476.
- (47) Peled, E.; Bar Tow, D.; Merson, A.; Gladkikh, A.; Burstein, L.; Golodnitsky, D. *J. Power Sources* **2001**, *97–98*, 52.
- (48) Abe, K.; Miyoshi, K.; Hattori, T.; Ushigoe, Y.; Yoshitake, H. *J. Power Sources* **2008**, *184*, 449.